

Anomalous Hall effect in kagome ferromagnet MgMn6Sn6 single crystal

Zhonghua Ma(马中华), Jie Du(杜杰), Jianhua Wang(王建华), Feng Zhou(周凤), Jie Chen(陈杰), Tao Zhu(朱涛), Hang Li(李航), and Wenhong Wang(王文洪)

Citation: Chin. Phys. B, 2026, 35 (**2**): 027302. DOI: 10.1088/1674-1056/adf4a4
http://cpb.iphy.ac.cn; http://iopscience.iop.org/cpb

What follows is a list of articles you may be interested in

Magnetic and electrical transport properties in GdAlSi and SmAlGe

Jing Gong(巩静), Huan Wang(王欢), Xiao-Ping Ma(马小平), Xiang-Yu Zeng(曾祥雨), Jun-Fa Lin(林浚发), Kun Han(韩坤), Yi-Ting Wang(王乙婷), and Tian-Long Xia(夏天龙)

Chin. Phys. B, 2024, 33 (**7**): 077302. DOI: 10.1088/1674-1056/ad41ba

Nonmonotonic anomalous Hall effect and anisotropic magnetoresistance in SrRuO3/PbZr0.52Ti0.48O3 heterostructures

Zhen-Li Wang(王振礼), Chao-Yang Kang(康朝阳), Cai-Hong Jia(贾彩虹), Hai-Zhong Guo(郭海中), and Wei-Feng Zhang(张伟风)

Chin. Phys. B, 2023, 32 (**10**): 107303. DOI: 10.1088/1674-1056/accd58

Electric modulation of anisotropic magnetoresistance in Pt/HfO2-x/NiOy/Ni heterojunctions

Xiaoyu Ye(叶晓羽), Xiaojian Zhu(朱小健), Huali Yang(杨华礼), Jipeng Duan(段吉鹏), Cui Sun(孙翠), and Run-Wei Li(李润伟)

Chin. Phys. B, 2023, 32 (**8**): 087305. DOI: 10.1088/1674-1056/acd2b6

Negative magnetoresistance in Dirac semimetal Cd3As2 with in-plane magnetic field perpendicular to current

Hao-Nan Cui(崔浩楠), Guang-Yu Zhu(祝光宇), Jian-Kun Wang(王建坤), Jia-Jie Yang(杨佳洁), Wen-Zhuang Zheng(郑文壮), Ben-Chuan Lin(林本川), Zhi-Min Liao(廖志敏), Shuo Wang(王硕), and Da-Peng Yu(俞大鹏)

Chin. Phys. B, 2023, 32 (**7**): 077305. DOI: 10.1088/1674-1056/accd50

Analytical formula describing the non-saturating linear magnetoresistance in inhomogeneous conductors

Shan-Shan Chen(陈珊珊), Yang Yang(杨阳), and Fan Yang(杨帆)

Chin. Phys. B, 2022, 31 (**8**): 087303. DOI: 10.1088/1674-1056/ac6582

Anomalous Hall effect in kagome ferromagnet $MgMn_6Sn_6$ single crystal

Zhonghua Ma(马中华)[1], Jie Du(杜杰)[2], Jianhua Wang(王建华)[2], Feng Zhou(周凤)[1], Jie Chen(陈杰)[1], Tao Zhu(朱涛)[1], Hang Li(李航)[1,†], and Wenhong Wang(王文洪)[1]

[1] *Institute of Quantum Materials and Devices, School of Electronics and Information Engineering, Tiangong University, Tianjin* 300387, *China*
[2] *School of Material Science and Engineering, Tiangong University, Tianjin* 300387, *China*

(Received 27 April 2025; revised manuscript received 11 July 2025; accepted manuscript online 28 July 2025)

Kagome magnets are of growing interest due to their topological electronic structures and unconventional magnetic behavior. Here, we report on the anomalous Hall effect (AHE) in the kagome ferromagnet $MgMn_6Sn_6$, which has a Curie temperature of ~ 290 K and an in-plane easy magnetization axis. Magnetotransport measurements show a positive magnetoresistance (*MR*) below 50 K, which becomes negative at higher temperatures. An intrinsic anomalous Hall conductivity of 114 S·cm^{-1} is observed in $MgMn_6Sn_6$ single crystals, consistent with *ab initio* calculations. Moreover, theoretical predictions indicate that shifting the Fermi level (E_F) upward by ~ 70 meV could enhance the AHE to ~ 528 S·cm^{-1}. These results position $MgMn_6Sn_6$ as a promising and tunable platform for exploring topological magnetism and related electronic phenomena.

Keywords: magnetoresistance, kagome ferromagnet, anomalous Hall effect

PACS: 73.43.Qt, 75.50.Cc, 75.47.–m

DOI: 10.1088/1674-1056/adf4a4 **CSTR:** 32038.14.CPB.adf4a4

1. Introduction

The kagome lattice has attracted significant interest in the field of topological materials due to its unique corner-sharing triangular atomic arrangement. This geometry gives rise to non-trivial electronic and spin structures, such as flat band,[1] Dirac/Weyl points,[2,3] and magnetic skyrmions.[4,5] Theoretical studies suggest that these features are key sources of Berry curvature,[6,7] which acts as a fictitious magnetic field, leading to prominent magneto-electric responses such as the anomalous Hall effect (AHE),[8] anomalous Nernst effect (ANE),[9–11] and topological Hall effect (THE).[12] Over the past decade, a wide range of magnetic kagome systems based on transition metal atoms have demonstrated diverse topological properties. These include ferromagnets such as Fe_3Sn_2,[2,13] and $Co_3Sn_2S_2$,[3,14] antiferromagnets like Mn_3X (X = Ga/Ge/Sn),[15–18] and FeGe,[19] and no-resolvable magnetic order AV_3Sb_5 (A = alkali metal).[20–24] These findings establish the kagome lattice as a compelling platform for exploring the topological properties in magnet materials.

Recently, Mn-based kagome compounds with the formula RMn_6X_6 (R = rareearth elements, X = main-group elements) have garnered increasing attention due to their rich magnetic structures and intriguing transport properties.[25] For instance, room-temperature topological magnetic skyrmions have been observed in $TbMn_6Sn_6$,[5] while pronounced anomalous Hall effect (AHE) and anomalous Nernst effect (ANE) have been reported in several compounds, including the ferrimagnet $GdMn_6Sn_6$,[26] the ferromagnet $LiMn_6Sn_6$,[26] and the helical antiferromagnet YMn_6Sn_6.[9] Furthermore, recent angle-resolved photoemission spectroscopy (ARPES) and scanning tunneling microscopy (STM) studies have revealed key electronic features, such as Dirac cones, flat bands, and saddle points, in YMn_6Sn_6[27] and identified intrinsic Chern quantum phases in the out-of-plane ferrimagnet $TbMn_6Sn_6$.[28] The presence of a pure Mn-based kagome lattice, along with the tunability offered by substituting rare-earth and main-group elements,[29–31] makes RMn_6X_6 compounds an exceptional platform for exploring and engineering topological phenomena in kagome systems.

In this study, we focus on the Mn-based kagome compound $MgMn_6Sn_6$, in which the alkaline-earth element Mg forms a honeycomb framework, while the Mn atoms construct a kagome lattice that contributes to the system's magnetic moment. Recent investigations have systematically explored the magnetocaloric effect (MCE)[32] and electronic band structure[33] of $MgMn_6Sn_6$ through experimental and *ab initio* calculations, respectively. These studies revealed that the easy axis of magnetization lies within the *ab*-plane and that various topological band features, such as Dirac fermions, van Hove singularities, and flat band, emerge near the Fermi level (E_F). Here, we systematically investigate the electrical transport properties of $MgMn_6Sn_6$ single crystal. Our measurements show that the magnetoresistance (*MR*) is positive below 50 K but gradually turns negative as the temperature in-

†Corresponding author. E-mail: hangli@tiangong.edu.cn

© 2026 Chinese Physical Society and IOP Publishing Ltd. All rights, including for text and data mining, AI training, and similar technologies, are reserved.

creases. The intrinsic anomalous Hall conductivity (AHC) is measured to be approximately 114 S·cm^{-1}. Notably, *ab initio* calculations predict an energy-dependent AHC that exhibits a broad peak approximately 70 meV above E_F, suggesting that the AHC can be enhanced to around 528 S·cm^{-1} by tuning the E_F through methods such as pressure application[34,35] or doping.[36] These results indicate that $MgMn_6Sn_6$ is a potential tunable ferromagnetic topological material candidate.

2. Experimental methods

$MgMn_6Sn_6$ single crystals were synthesized using the Sn self-flux method.[32] High-purity magnesium (99.99%), manganese (99.95%), and tin (99.999%) spheres were weighed in a molar ratio of 4:1:8 and loaded into an alumina crucible. The crucible was sealed in an evacuated quartz tube, which was then heated to 1073 K and held for 12 hours after an initial 6 hour ramp to ensure complete melting and homogeneous mixing of the elements. Following homogenization, the furnace was cooled at a controlled rate of 4 K/h down to 693 K. At this point, the excess tin flux was removed by centrifuge, yielding hexagonal plate-like single crystals, as shown in the inset of Fig. 1(c). Residual Sn adhered to the crystal surfaces was removed by mechanical polishing.

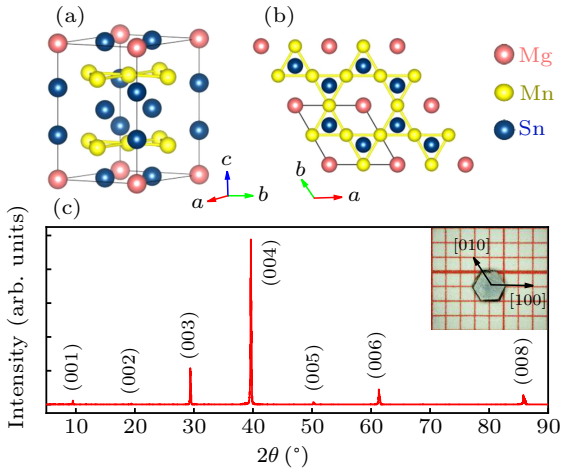


Fig. 1. (a) Schematic crystal structure of $MgMn_6Sn_6$. (b) Top view of the structure, highlighting the Mn atoms forming kagome lattices within the *ab*-plane. (c) The XRD pattern of the hexagonal plane of an $MgMn_6Sn_6$ single crystal measured at room temperature. The inset shows a photograph of a representative hexagonal plate-like $MgMn_6Sn_6$ single crystal obtained from Sn flux growth.

The elemental composition and crystallographic structure of the synthesized single crystals were characterized using energy-dispersive x-ray spectroscopy (EDS) and x-ray diffraction (XRD), respectively. Electrical transport and magnetic measurements were carried out using a physical property measurement system (PPMS, Quantum Design Dynacool). *Ab initio* calculations were performed using the Vienna *ab initio* Simulation Package (VASP),[27–29] employing the Perdew–Burke–Ernzerhof (PBE) generalized gradient approximation (GGA) for the exchange–correlation functional.[30] The plane-wave energy cutoff was set to 550 eV, and convergence criteria were defined as 10^{-6} eV for total energy and 0.01 eV·Å^{-1} for forces on ions. A $10 \times 10 \times 6$ Monkhorst–Pack *k*-point mesh was used for Brillouin zone sampling. The intrinsic anomalous Hall conductivity (AHC) was calculated using the Wannier90[31] and WannierTools[32] packages, based on maximally localized Wannier functions constructed from the DFT-calculated electronic structure.

3. Results and discussion

As shown in Fig. 1(a), $MgMn_6Sn_6$ crystallizes in a hexagonal $HfFe_6Ge_6$-type structure with the space group $P6/mmm$ (No. 191). Within a single unit cell, two Mn atomic layers (yellow spheres in Fig. 1(a)) are separated by three Sn layers (dark blue spheres in Fig. 1(a)). The crystal structure of $MgMn_6Sn_6$ is characterized by the lattice parameters $a = b = 5.517$ Å and $c = 9.032$ Å. In the top view in Fig. 1(b), the Mn atoms clearly form a kagome lattice within the *ab*-plane. The grown single crystals exhibit a well-defined hexagonal platelet morphology, typical of other "166" kagome compounds, as shown in the inset of Fig. 1(c).[37] EDS analysis confirms the elemental ratio as Mg:Mn:Sn = 7.82:45.79:46.39, which is in close agreement with the ideal 1:6:6 stoichiometry. The XRD pattern of the hexagonal plane, displayed in Fig. 1(c), shows only (00*l*) diffraction peaks, confirming that the broad surface of the single crystal corresponds to the (001) plane.

The upper panel of Fig. 2(a) shows the temperature-dependent magnetization $M(T)$ curves of $MgMn_6Sn_6$ measured from 5 K to 380 K under an applied magnetic field of $\mu_0 H = 0.01$ T along the *a*-axis ($H \parallel a$) and *c*-axis ($H \parallel c$). The lower panel of Fig. 2(a) displays the first derivative $\mathrm{d}M/\mathrm{d}T$ as a function of temperature, from which the Curie temperatures (T_C) are determined to be approximately 290 K for $H \parallel a$ and 293 K for $H \parallel c$. These values are consistent with previous polycrystalline data[38] and are slightly lower than those reported for earlier single-crystal studies.[32] Figures 2(b) and 2(c) present the isothermal magnetization $M(H)$ curves measured between 5 K and 340 K along the *a*-axes and *c*-axes, respectively. No magnetic hysteresis is observed along either direction, indicating soft ferromagnetic behavior. The $M(H)$ curves confirm that the easy magnetization direction lies in the *ab*-plane.

Figure 3(a) shows the temperature dependence of longitudinal resistivity curves $\rho_{xx}(T)$, exhibiting typical metallic behavior. The residual resistivity ratio [RRR = ρ_{xx} (300 K)/ρ_{xx} (2 K)] of 38.64 indicates the high crystalline quality of the grown $MgMn_6Sn_6$. Figure 3(b) presents the magnetoresistance curves, $MR = [\rho_{xx}(\mu_0 H) - \rho_{xx}(0)]/\rho_{xx}(0)$. At temperature $T \leq 50$ K, the *MR* is positive and gradually decreases

with increasing temperature. The maximum *MR* reaches approximately 13% at $T = 5$ K and $\mu_0 H = 5$ T. At $T = 50$ K, *MR* above the saturation field (H_S) begins to transition from positive to negative. For $T > 50$ K, the *MR* above H_S becomes increasingly negative, while remaining positive at lower magnetic fields. When T exceeds 100 K, *MR* is negative across the entire field range. At low temperatures, *MR* curves exhibit a kink around 2 T and show an almost linear increase at higher fields, similar to behavior observed in $LiMn_6Sn_6$.[39] The *MR* in magnetic materials is influenced by various factors. Generally, positive *MR* can be attributed to the Lorentz force, weak anti-localization effect,[40] n–p compensation band structure,[41] and non-trivial band structure.[42] negative *MR*, on the other hand, may arise from spin-dependent electron scattering in all magnetic materials[43] or the chiral anomaly in Weyl semimetals,[44] Considering the characteristics of these factors and the *MR* curves of $MgMn_6Sn_6$, we think that the sign change in *MR* in $MgMn_6Sn_6$ results from the competition between the positive *MR* induced by the Lorentz force and the non-trivial band structure near the Fermi level[33] and the negative *MR* due to spin-dependent electron scattering with temperature. The turning points observed at low magnetic fields are likely caused by magnetic domain transformations.[45]

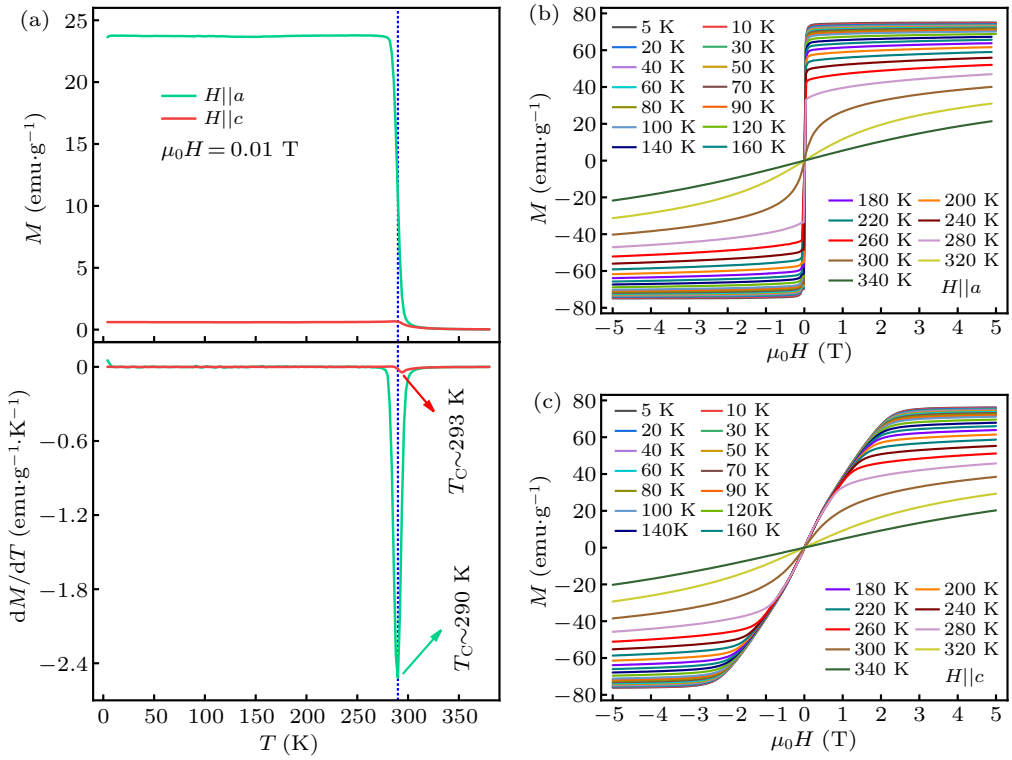


Fig. 2. Magnetic characterization of $MgMn_6Sn_6$ single crystals measured with magnetic field applied parallel to the *a*-axis ($H \parallel a$) and *c*-axis ($H \parallel c$), respectively. (a) Temperature dependence of magnetization $M(T)$ measured under a magnetic field of $\mu_0 H = 0.01$ T, along with the corresponding dM/dT curves. The blue dashed line marks the Curie temperature T_C. (b) and (c) Isothermal magnetization $M(H)$ curves recorded at various temperatures ranging from 5 K and 340 K, showing the magnetic anisotropy between the in-plane and out-of-plane directions.

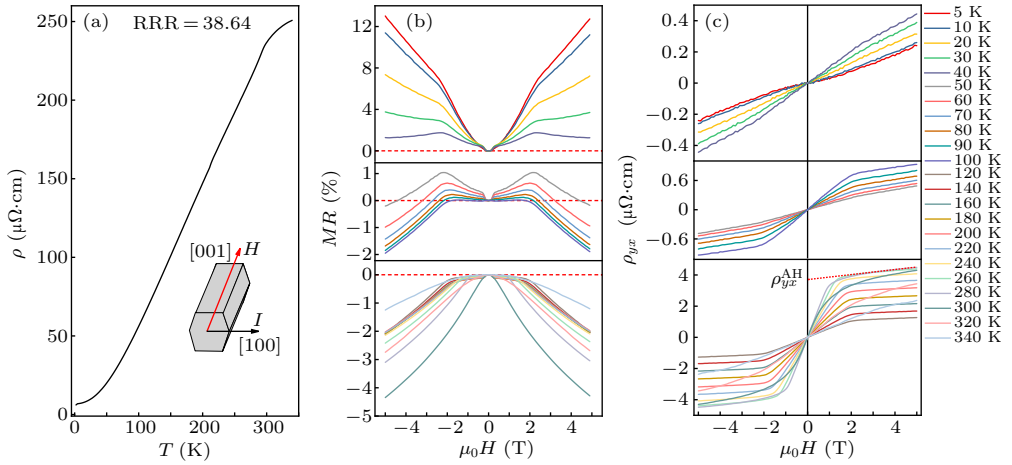


Fig. 3. Electrical transport properties of $MgMn_6Sn_6$ single crystals with current applied along [100] ($I \parallel [100]$) and magnetic field along [001] ($H \parallel [001]$). (a) Temperature dependence of longitudinal resistivity $\rho_{xx}(T)$. The inset illustrates the measurement configuration of current and magnetic field directions. (b) Field dependence of magnetoresistance (*MR*) at various temperatures. (c) Field dependence of Hall resistivity ρ_{yx} at different temperatures.

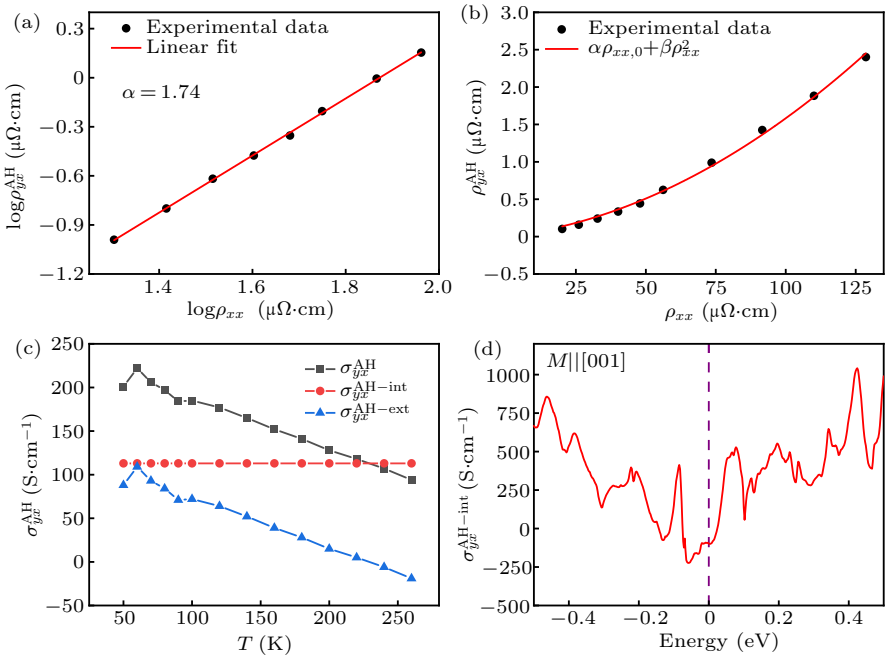


Fig. 4. Characterization of anomalous Hall effect in $MgMn_6Sn_6$ single crystals. (a) Plot of $\log\rho_{yx}^{AH}$ versus $\log\rho_{xx}$. The black points represent experimental data, and the red line indicates the linear fit. (b) Analysis of the anomalous Hall effect mechanism through ρ_{yx}^{AH} versus ρ_{xx}. Black points represent the experimental data, the red line is the fitting curve based on Jin's model.[47] (c) Temperature dependence of anomalous Hall conductivity contributions from different mechanisms. (d) Energy dependence of the intrinsic anomalous Hall conductivity σ_{yx}^{AH-int} of $MgMn_6Sn_6$ single crystals with moment along [001].

Figure 3(c) shows the field dependence of the Hall resistivity ρ_{yx} over a temperature range from 5 K to 340 K. The ρ_{yx} curves also exhibit distinct characteristics around 50 K. At low temperatures ($T = 5$ K and 10 K), ρ_{yx} curves exhibit a small slope in the low-field region, followed by a weak increase for $H > H_S$. For 10 K $< T <$ 50 K, the ρ_{yx} curves vary almost linearly with the applied magnetic field. For $T \geq 50$ K, a typical anomalous Hall effect is observed. The maximum value of ρ_{yx} is observed at 260 K. The Hall resistivity ρ_{yx} is given by

$$\rho_{yx} = R_0 B + 4\pi R_S M, \tag{1}$$

where R_0 and R_S denote the normal and anomalous Hall coefficients, respectively. The term $R_0 B$ represents the normal Hall effect ρ_{yx}^{NH}, while the second term of Eq. (1) corresponds to the anomalous Hall contribution ρ_{yx}^{AH}.[46] Once the magnetization saturates under an applied field, the ρ_{yx}^{AH} remains constant. Therefore, it can be extracted by performing a linear fit to the ρ_{yx} curves in the high-field region beyond saturation, as indicated by the red dotted line in Fig. 3(c). The slope and intercept of this linear fit yield R_0 and ρ_{yx}^{AH}, respectively.

To elucidate the origin of the AHE in $MgMn_6Sn_6$, we analyzed the relationship between $\log\rho_{yx}^{AH}$ and $\log\rho_{xx}$, as illustrated in Fig. 4(a). The linear fit yields a slope of $\alpha = 1.74$, suggesting a dominant contribution from intrinsic mechanisms. To further clarify the AHE mechanism, we fitted the experimental data above 50 K using the following expression:[47]

$$\rho_{yx}^{AH} = \alpha\rho_{xx,0} + \beta\rho_{xx}^2, \tag{2}$$

where the two terms represent extrinsic and intrinsic contributions, respectively. As shown in Fig. 4(b), the fitting curve obtained from Eq. (2) exhibits excellent agreement with the experimental data. According to the curve fitting results of Fig. 4(b), the different contributions of the anomalous Hall conductivity σ_{yx}^{AH} can be separated, which can be calculated using the following equation:

$$\sigma_{yx}^{AH} = \frac{\rho_{yx}^{AH}}{(\rho_{yx}^{AH})^2 + \rho_{xx}^2}. \tag{3}$$

The results, presented in Fig. 4(c), reveal that the intrinsic contribution (σ_{yx}^{AH-int}) is ~ 114 S·cm^{-1}, which is comparable to that reported for $HoMn_6Sn_6$ (~ 120 S·cm^{-1}).[48] Additionally, our *ab initio* calculations, as shown in Fig. 4(d), predict an intrinsic anomalous Hall conductivity of 98 S·cm^{-1} at E_F with moment along [001], in good agreement with experimental observations. Notably, a pronounced peak appears at ~ 70 meV above E_F, suggesting that electron doping could enhance the intrinsic AHC to 528 S·cm^{-1}.

In summary, we have systematically investigated the magnetic and transport properties of $MgMn_6Sn_6$, a ferromagnet with a Curie temperature of 290 K and easy magnetization direction within the *ab* plane. A sign reversal in the *MR* near 50 K is observed, arising from the competition between negative *MR* (due to suppressed spin-disorder scattering) and positive *MR* (attributed to the Lorentz force). Our measurements confirm that the intrinsic AHE mechanism dominates, yielding a robust anomalous Hall conductivity of ~ 114 S·cm^{-1} that remains stable across a wide temperature range, a signature of persistent Berry curvature in the occupied states. Furthermore, *ab initio* calculations corroborate these findings, predicting a

substantial intrinsic AHC (~ 98 S·cm^{-1}) near E_F and a dramatic enhancement to ~ 528 S·cm^{-1} at ~ 70 meV above E_F. These results highlight $MgMn_6Sn_6$ as a promising platform for engineering topological states in magnetic kagome systems.

Acknowledgements

Project supported by the National Natural Science Foundation of China (Grant No. 12204347), National Key Research and Development Program of China (Grant No. 2022YFA1402600), and the Fund from Beijing National Laboratory for Condensed Matter Physics (Grant No. 2023BNLCMPKF011). A portion of this work was carried out at the Synergetic Extreme Condition User Facility (SECUF) in Huairou Science City.

References

[1] Lin Z, Choi J H, Zhang Q, Qin W, Yi S, Wang P, Li L, Wang Y, Zhang H, Sun Z, Wei L, Zhang S, Guo T, Lu Q, Cho J H, Zeng C and Zhang Z 2018 *Phys. Rev. Lett.* **121** 96401

[2] Ye L, Kang M, Liu J, Von Cube F, Wicker C R, Suzuki T, Jozwiak C, Bostwick A, Rotenberg E, Bell D C, Fu L, Comin R and Checkelsky J G 2018 *Nature* **555** 638

[3] Liu D F, Liang A J, Liu E K, Xu Q N, Li Y W, Chen C, Pei D, Shi W J, Mo S K, Dudin P, Kim T, Cacho C, Li G, Sun Y, Yang L X, Liu Z K, Parkin S S P, Felser C and Chen Y L 2019 *Science* **365** 1282

[4] Hou Z, Ren W, Ding B, Xu G, Wang Y, Yang B, Zhang Q, Zhang Y, Liu E, Xu F, Wang W, Wu G, Zhang X, Shen B and Zhang Z 2017 *Adv. Mater.* **29** 1701144

[5] Li Z, Yin Q, Jiang Y, Zhu Z, Gao Y, Wang S, Shen J, Zhao T, Cai J, Lei H, Lin S, Zhang Y and Shen B 2023 *Adv. Mater.* **35** 2211164

[6] Xiao D, Chang M C and Niu Q 2010 *Rev. Mod. Phys.* **82** 1959

[7] Neubauer A, Pfleiderer C, Binz B, Rosch A, Ritz R, Niklowitz P G and Böni P 2009 *Phys. Rev. Lett.* **102** 186602

[8] Liu E, Sun Y, Kumar N, Muechler L, Sun A, Jiao L, Yang S-Y, Liu D, Liang A, Xu Q, Kroder J, Süß V, Borrmann H, Shekhar C, Wang Z, Xi C, Wang W, Schnelle W, Wirth S, Chen Y, Goennenwein S T B and Felser C 2018 *Nat. Phys.* **14** 1125

[9] Roychowdhury S, Ochs A M, Guin S N, Samanta K, Noky J, Shekhar C, Vergniory M G, Goldberger J E and Felser C 2022 *Adv. Mater.* **34** 2201350

[10] Xu X, Yin J X, Ma W, Tien H J, Qiang X B, Reddy P V S, Zhou H, Shen J, Lu H Z, Chang T R, Qu Z and Jia S 2022 *Nat. Commun.* **13** 1197

[11] Zhang H, Koo J, Xu C, Sretenovic M, Yan B and Ke X 2022 *Nat. Commun.* **13** 1091

[12] Li H, Ding B, Chen J, Li Z, Hou Z, Liu E, Zhang H, Xi X, Wu G and Wang W 2019 *Appl. Phys. Lett.* **114** 192408

[13] Yin J X, Zhang S S, Li H, Jiang K, Chang G, Zhang B, Lian B, Xiang C, Belopolski I, Zheng H, Cochran T A, Xu S Y, Bian G, Liu K, Chang T R, Lin H, Lu Z Y, Wang Z, Jia S, Wang W and Hasan M Z 2018 *Nature* **562** 91

[14] Morali N, Batabyal R, Nag P K, Liu E, Xu Q, Sun Y, Yan B, Felser C, Avraham N and Beidenkopf H 2019 *Science* **365** 1286

[15] Nakatsuji S, Kiyohara N and Higo T 2015 *Nature* **527** 212

[16] Ikhlas M, Tomita T, Koretsune T, Suzuki M T, Nishio-Hamane D, Arita R, Otani Y and Nakatsuji S 2017 *Nat. Phys.* **13** 1085

[17] Chen T, Tomita T, Minami S, Fu M, Koretsune T, Kitatani M, Muhammad I, Nishio-Hamane D, Ishii R, Ishii F, Arita R and Nakatsuji S 2021 *Nat. Commun.* **12** 572

[18] Song L, Zhou F, Li H, Ding B, Li X, Xi X, Yao Y, Lau Y and Wang W 2024 *Adv. Funct. Mater.* **34** 2316588

[19] Teng X, Chen L, Ye F, Rosenberg E, Liu Z, Yin J X, Jiang Y X, Oh J S, Hasan M Z, Neubauer K J, Gao B, Xie Y, Hashimoto M, Lu D, Jozwiak C, Bostwick A, Rotenberg E, Birgeneau R J, Chu J H, Yi M and Dai P 2022 *Nature* **609** 490

[20] Zhao H, Li H, Ortiz B R, Teicher S M L, Park T, Ye M, Wang Z, Balents L, Wilson S D and Zeljkovic I 2021 *Nature* **599** 216

[21] Nie L, Sun K, Ma W, Song D, Zheng L, Liang Z, Wu P, Yu F, Li J, Shan M, Zhao D, Li S, Kang B, Wu Z, Zhou Y, Liu K, Xiang Z, Ying J, Wang Z, Wu T and Chen X 2022 *Nature* **604** 59

[22] Zhong Y, Liu J, Wu X, Guguchia Z, Yin J X, Mine A, Li Y, Najafzadeh S, Das D, Mielke C, Khasanov R, Luetkens H, Suzuki T, Liu K, Han X, Kondo T, Hu J, Shin S, Wang Z, Shi X, Yao Y and Okazaki K 2023 *Nature* **617** 488

[23] Deng H, Qin H, Liu G, Yang T, Fu R, Zhang Z, Wu X, Wang Z, Shi Y, Liu J, Liu H, Yan X Y, Song W, Xu X, Zhao Y, Yi M, Xu G, Hohmann H, Holbæk S C, Dürrnagel M, Zhou S, Chang G, Yao Y, Wang Q, Guguchia Z, Neupert T, Thomale R, Fischer M H and Yin J X 2024 *Nature* **632** 775

[24] Liu Y, Liu Z Y, Bao J K, Yang P T, Ji L W, Wu S Q, Shen Q X, Luo J, Yang J, Liu J Y, Xu C C, Yang W Z, Chai W L, Lu J Y, Liu C C, Wang B S, Jiang H, Tao Q, Ren Z, Xu X F, Cao C, Xu Z A, Zhou R, Cheng J G and Cao G H 2024 *Nature* **632** 1032

[25] Xu X, Yin J X, Qu Z and Jia S 2023 *Rep. Prog. Phys.* **86** 114502

[26] Asaba T, Thomas S M, Curtis M, Thompson J D, Bauer E D and Ronning F 2020 *Phys. Rev. B* **101** 174415

[27] Li M, Wang Q, Wang G, Yuan Z, Song W, Lou R, Liu Z, Huang Y, Liu Z, Lei H, Yin Z and Wang S 2021 *Nat. Commun.* **12** 3129

[28] Yin J X, Ma W, Cochran T A, Xu X, Zhang S S, Tien H J, Shumiya N, Cheng G, Jiang K, Lian B, Song Z, Chang G, Belopolski I, Multer D, Litskevich M, Cheng Z J, Yang X P, Swidler B, Zhou H, Lin H, Neupert T, Wang Z, Yao N, Chang T R, Jia S and Zahid Hasan M 2020 *Nature* **583** 533

[29] Ma W, Xu X, Yin J X, Yang H, Zhou H, Cheng Z J, Huang Y, Qu Z, Wang F, Hasan M Z and Jia S 2021 *Phys. Rev. Lett.* **126** 246602

[30] Zhu Y, Zhang D, Zheng G, Chen K W, Bhandari H, Jenkins K, Chan A, Ghimire N J and Li L 2024 *Phys. Rev. B* **110** 195125

[31] Lv B, Zhong R, Luo X, Ma S, Chen C, Wang S, Luo Q, Gao F, Fang C and Ren W 2025 *Scr. Mater.* **255** 116345

[32] Song Z, Chen Z, Kan X, Wang S, Wang M, Zheng G and Ma Y 2024 *Mater. Today Phys.* **46** 101493

[33] Sau J, Banerjee H, Saha S, Kumar N and Kumar M 2024 arXiv: 2408.02504.

[34] Kong X, Tao Z, Zhang R, Xia W, Chen X, Pei C, Ying T, Qi Y, Guo Y, Yang X and Li S 2024 *Chin. Phys. Lett.* **41** 047503

[35] Gao L, Lai J, Chen D, Pei C, Wang Q, Zhao Y, Li C, Cao W, Wu J, Chen Y, Chen X, Sun Y, Felser C and Qi Y 2024 *Chin. Phys. Lett.* **41** 057302

[36] Li L, Chi S, Ma W, Guo K, Xu G and Jia S 2024 *Chin. Phys. B* **33** 057501

[37] Wu H, Liu J, Li Y, Zhu P, Yang L, Chen F, Hu D and Wang Z 2024 *Chin. Phys. B* **33** 098101

[38] Mazet T, Venturini G, Welter R and Malaman B 1998 *J. Alloys Compd.* **264** 71

[39] Chen D, Le C, Fu C, Lin H, Schnelle W, Sun Y and Felser C 2021 *Phys. Rev. B* **103** 144410

[40] Wu X, Li X, Song Z, Berger C and De Heer W A 2007 *Phys. Rev. Lett.* **98** 136801

[41] Ali M N, Xiong J, Flynn S, Tao J, Gibson Q D, Schoop L M, Liang T, Haldolaarachchige N, Hirschberger M, Ong N P and Cava R J 2014 *Nature* **514** 205

[42] Liang T, Gibson Q, Ali M N, Liu M, Cava R J and Ong N P 2014 *Nat. Mater.* **14** 280

[43] Van Peski-Tinbergen T and Dekker A J 1963 *Physica* **29** 917

[44] Xiong J, Kushwaha S K, Liang T, Krizan J W, Hirschberger M, Wang W, Cava R J and Ong N P 2015 *Science* **350** 413

[45] Berger L 1978 *J. Appl. Phys.* **49** 2156

[46] Nagaosa N, Sinova J, Onoda S, MacDonald A H and Ong N P 2010 *Rev. Mod. Phys.* **82** 1539

[47] Tian Y, Ye L and Jin X 2009 *Phys. Rev. Lett.* **103** 87206

[48] Zeng H, Yu G, Luo X, Chen C, Fang C, Ma S, Mo Z, Shen J, Yuan M and Zhong Z 2022 *J. Alloys Compd.* **899** 163356